

**Mechanisms underlying the cerebellar deficits produced by repeated cannabis exposure**

Laura Cutando<sup>1</sup>, Arnau Busquets-Garcia<sup>1</sup>, Emma Puighermanal<sup>1</sup>, Maria Gomis-González<sup>1</sup>, José María Delgado-García<sup>2</sup>, Agnès Gruart<sup>2</sup>, Rafael Maldonado<sup>1</sup>, Andrés Ozaita<sup>1\*</sup>.

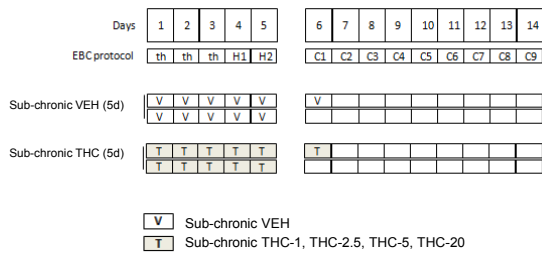
<sup>1</sup>Laboratori de Neurofarmacologia. Facultat de Ciències de la Salut i de la Vida. Universitat Pompeu Fabra, Barcelona, Spain.

<sup>2</sup>División de Neurociencias, Universidad Pablo de Olavide, Sevilla, Spain.

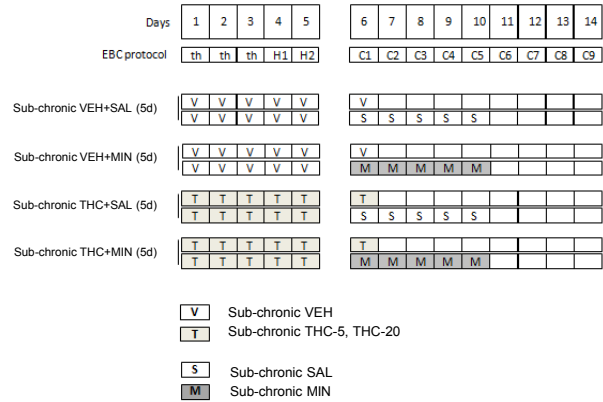
\*Corresponding author:

Andrés Ozaita, Laboratori de Neurofarmacologia, Facultat de Ciències de la Salut i de la Vida, Universitat Pompeu Fabra, Parc de Recerca Biomèdica de Barcelona, C/ Doctor Aiguader 88, 08003 Barcelona, Spain. Phone: +34-93-3160823; Fax: +34-93-3160901; e-mail: andres.ozaita@upf.edu

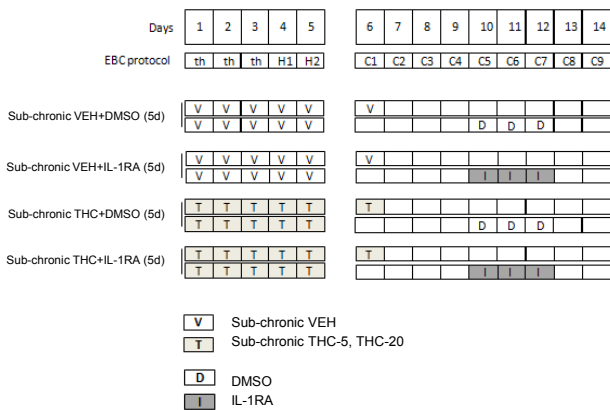
**A**



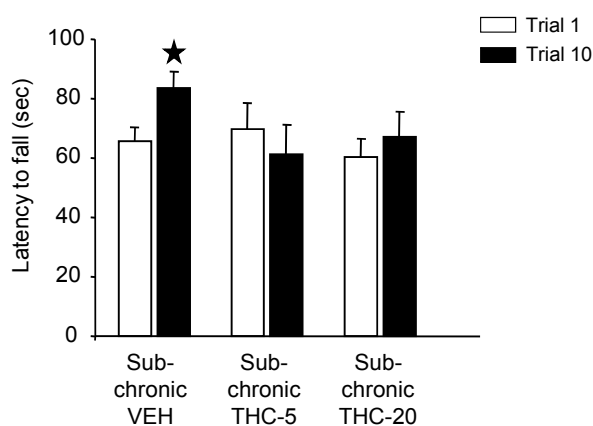
**B**



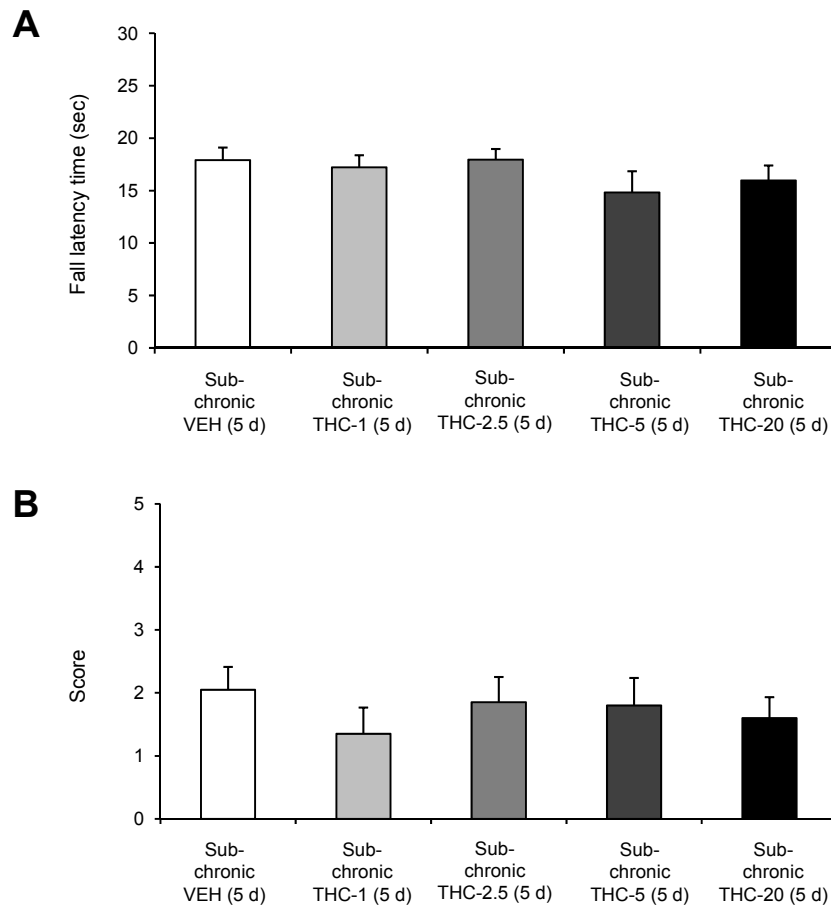
**C**



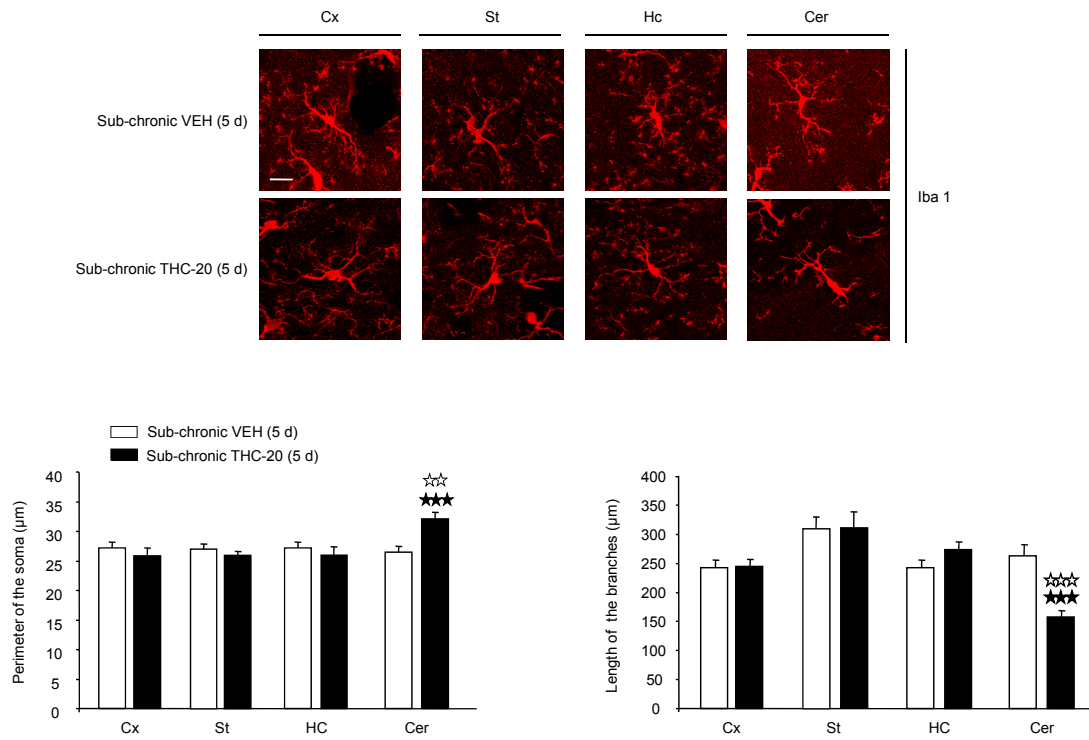
**Supplemental Figure 1.** Eyeblink conditioning schedules. (A) Chronogram for the experiment in Figure 1A. (B) Chronogram for experiment in Figure 4, A and C. (C) Chronogram for experiment in Figure 6A. Abbreviations: th, Search for thresholds; H, Habituation phase; C, Conditioning phase; T, THC; V, vehicle (VEH), M, minocycline (MIN); S, saline (SAL); I, IL-1RA; D, DMSO.



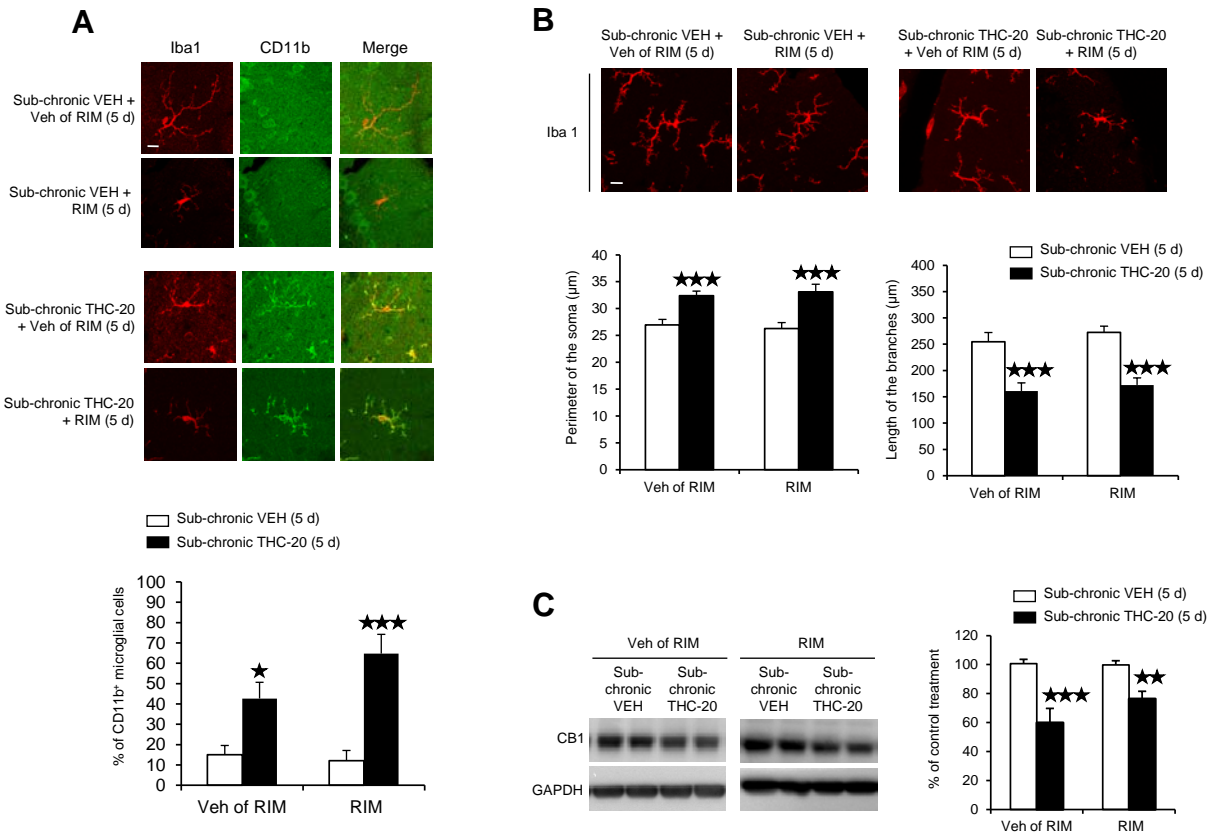
**Supplemental Figure 2.** Motor coordination performance in the accelerating rotarod after sub-chronic THC exposure. Mice were tested 5 d after the end of treatments with vehicle (sub-chronic VEH), THC (5 mg/kg) (sub-chronic THC-5) and THC (20 mg/kg) (sub-chronic THC-20). The latency to fall in the first trial (Trial 1) and on the tenth trial (Trial 10) of the accelerating rotarod is represented. Mice exposed to THC ( $n=8-10$  per group) showed a similar latency to fall in the first and tenth trial of the test session, while VEH-treated mice did improve in their performance. Data were expressed as mean  $\pm$  SEM. ★ $p<0.05$  vs. first trial.



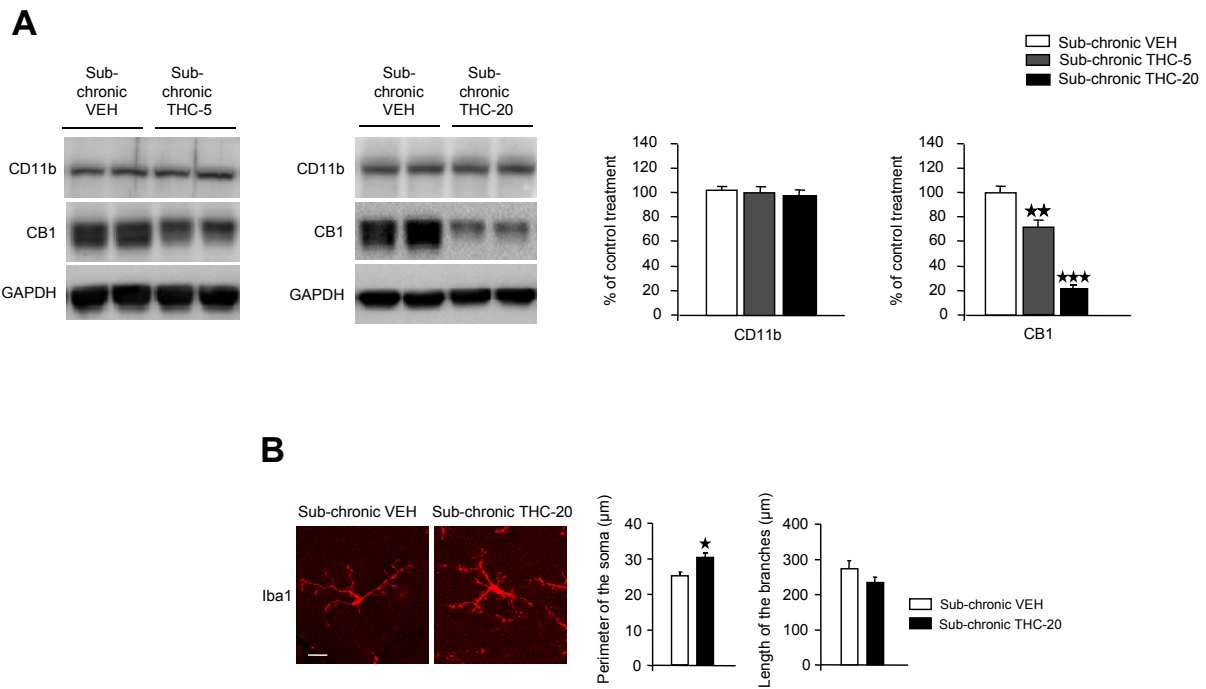
**Supplemental Figure 3.** Assessment of the equilibrium performance of mice 5 d after THC treatment cessation in the rod test. Mice ( $n=10$  per group) treated with VEH or THC (1, 2.5, 5, 20 mg/kg, i.p.) were tested in the rod test 5 d after the last VEH or THC administration. Results are displayed as fall latency (**A**) or score (**B**). Data were expressed as mean  $\pm$  SEM.



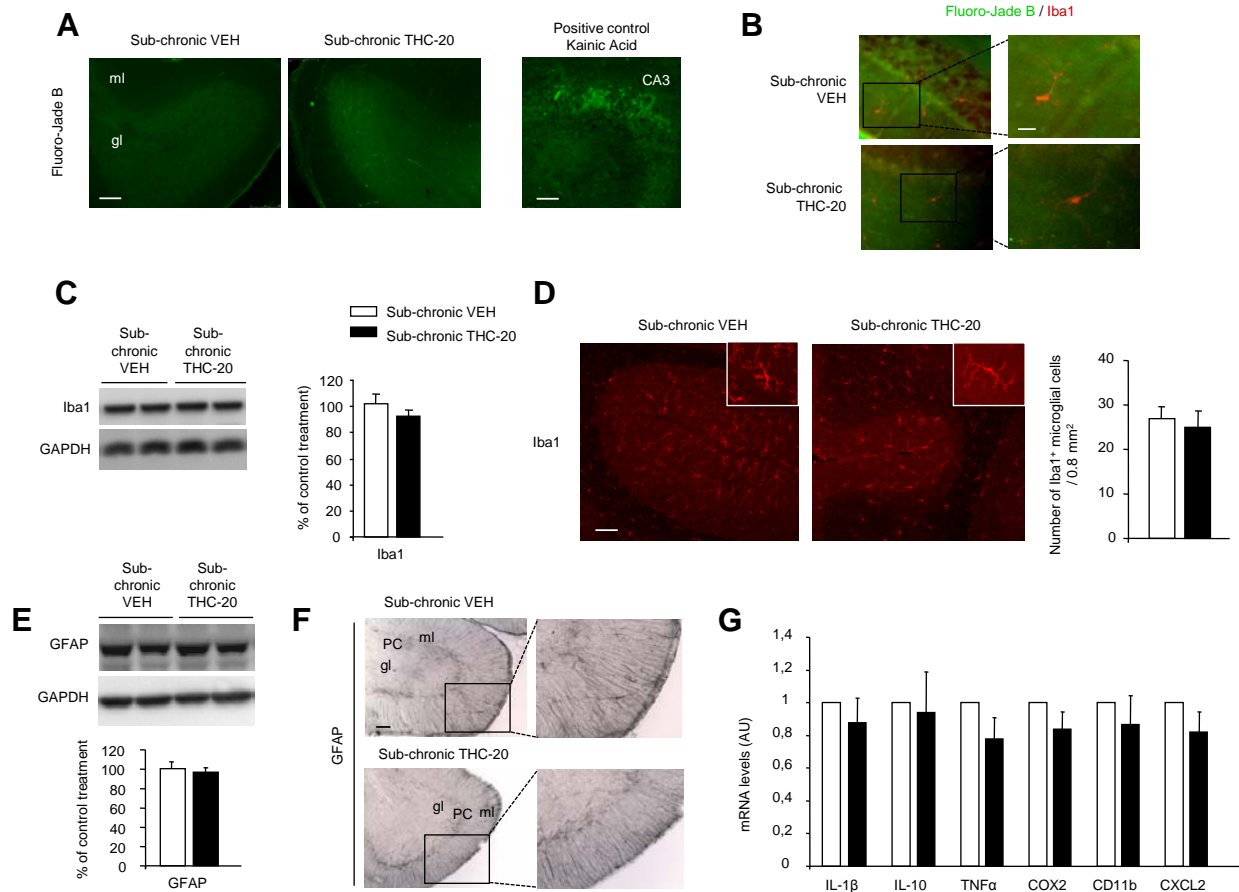
**Supplemental Figure 4.** Microglial activation 5 d after sub-chronic THC treatment cessation occurs mainly in the cerebellum. Morphological analysis of Iba1+ microglial cells in cortex, striatum, hippocampus and cerebellum from mice treated sub-chronically with VEH or THC-20 and sacrificed 5 d after the last VEH or THC administration (sub-chronic VEH (5 d) or sub-chronic THC-20 (5 d) groups) ( $n=3-4$  mice per group, 5 cells per mouse). The perimeter of the cell soma and the length of the microglial branches from Iba1-stained cells were analyzed with the ImageJ software (see Supplemental Figure 17). Scale bar: 25 µm.



**Supplemental Figure 5.** The precipitated THC withdrawal similarly promotes the activation of microglial cells detected 5 d after the end of the sub-chronic THC treatment (20 mg/kg, i.p.). (A) Immunodetection of Iba1 (red) and CD11b (green) proteins in cerebellar sagittal sections from mice treated sub-chronically with VEH or THC-20 and receiving acutely rimonabant (RIM, 10 mg/kg, i.p.) or its vehicle ( $n=5$  mice per group). The percentage of Iba1+/CD11b+ microglial cells was computed from 25 images (5 images per animal). Scale bar: 25  $\mu$ m. (B) Morphological analysis of Iba1+ microglial cells in cerebellar cortex from mice treated sub-chronically with VEH + Veh of RIM (sub-chronic VEH + Veh of RIM (5 d) group), VEH + RIM (sub-chronic VEH + RIM (5 d) group), THC-20 + Veh of RIM (sub-chronic THC-20 + Veh of RIM (5 d) group) and THC-20 + RIM (sub-chronic THC-20 + RIM (5 d) group) ( $n=3-5$  mice per group, 5 cells per mouse). The perimeter of the cell soma and the length of the microglial branches from Iba1-stained cells were analyzed with the ImageJ software (Supplemental Figure 17). Scale bar: 25  $\mu$ m. (C) Immunoblot and quantification of CB1R in cerebellar homogenates from mice analyzed 5 d after receiving sub-chronically THC-20 or VEH and acutely RIM or its vehicle ( $n=5$  mice per group). The optical density for CB1R detection was referred to the detection of the housekeeping control GAPDH in the same samples. Data were compared between groups (sub-chronic THC-20 + Veh of RIM (5 d) vs. sub-chronic VEH + Veh of RIM (5 d), and sub-chronic THC-20 + RIM (5 d) vs. sub-chronic VEH + RIM (5 d)) using one-way ANOVA and were expressed as mean  $\pm$  SEM.  $\star p<0.05$ ,  $\star\star p<0.01$ ,  $\star\star\star p<0.001$ .



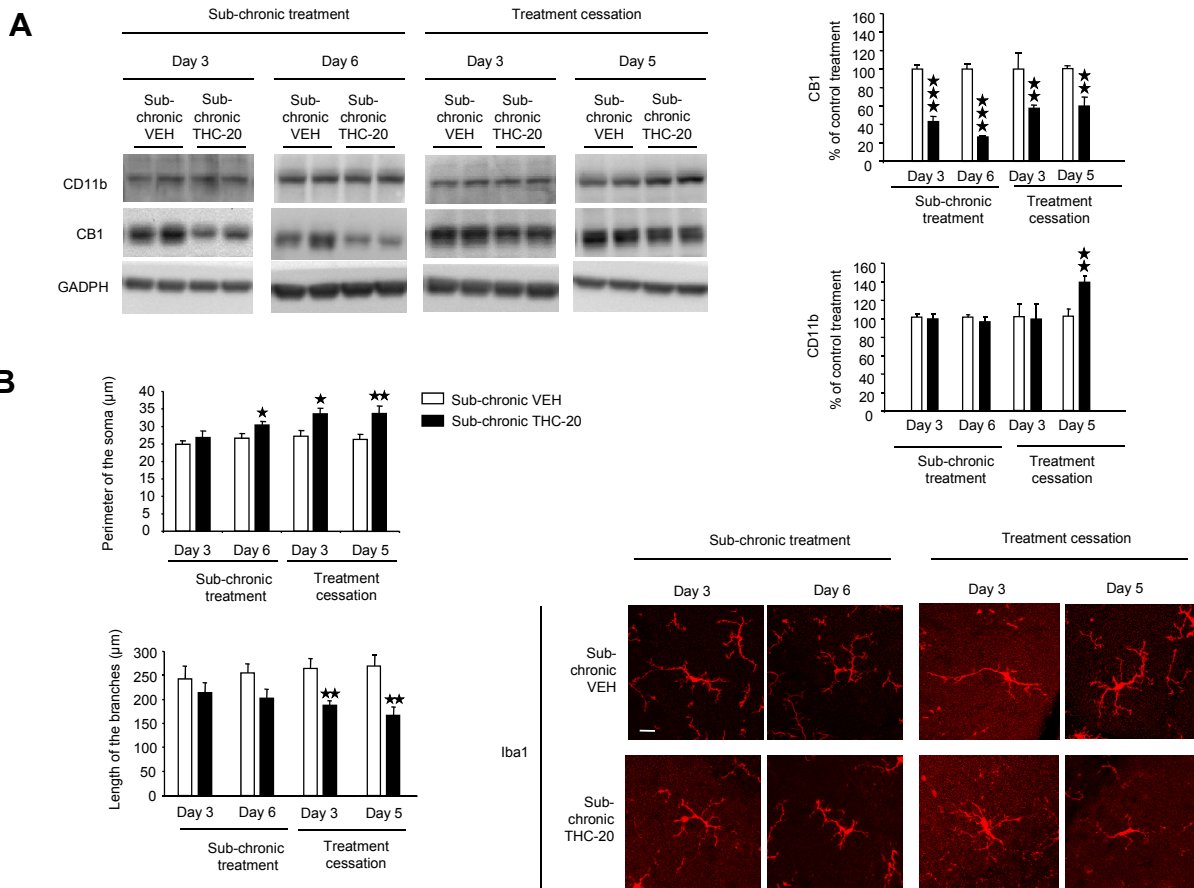
**Supplemental Figure 6.** Sub-chronic THC administration did not produce CD11b enhancement or a significant change in the microglial morphology. **(A)** Immunoblot and quantification of CD11b and CB1R in cerebellar homogenates from mice processed at the end of THC (5 or 20 mg/kg, i.p.) or VEH sub-chronic treatment ( $n=5$  mice per group). The optical density for CD11b and CB1R detection was referred to the detection of the housekeeping control GAPDH in the same samples. **(B)** Morphological analysis of Iba1+ microglial cells in the molecular layer of the cerebellum from mice treated sub-chronically with VEH or THC 20 mg/kg and sacrificed after 5 d ( $n=5$  mice per group, 5 cells per mouse). The perimeter of the cell soma and the length of the microglial branches from Iba1-stained cells were analyzed with the ImageJ software (Supplemental Figure 17). Scale bar: 25  $\mu\text{m}$ . Data were compared between groups using one-way ANOVA and expressed as mean  $\pm$  SEM. \* $p<0.05$ , \*\* $p<0.01$ , \*\*\* $p<0.001$ .



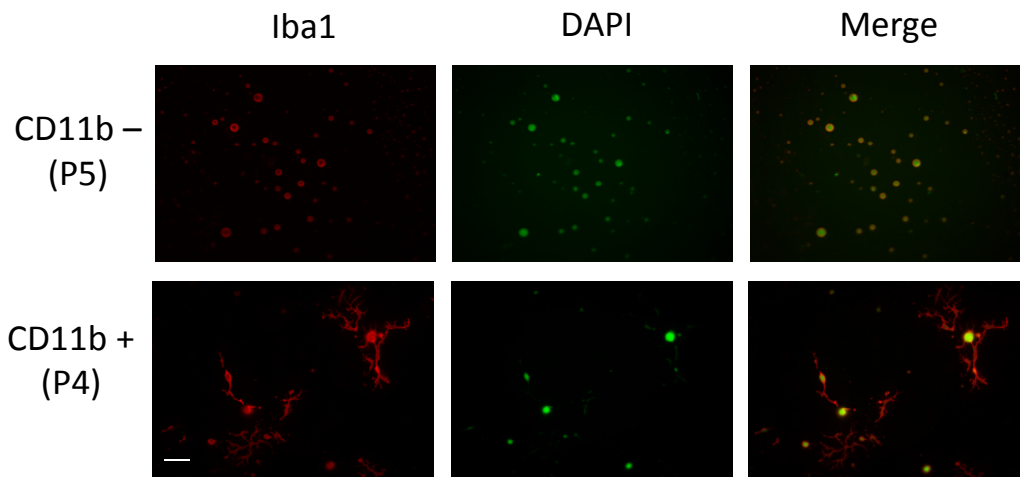
**Supplemental Figure 7.** No signs of cellular stress neither microglial or astroglial proliferation were detected at the end of the THC-20 sub-chronic treatment. **(A)** Brains were removed 30 min after the last THC-20 or VEH administration and processed for Fluoro-Jade B assay ( $n=4$  mice per group). As a positive control, an independent group of mice ( $n=3$  per group) was treated with an excitotoxic dose of kainic acid (15 mg/kg, i.p.) and their brains were processed for Fluoro-Jade B staining 3 d later. There was no sign of cellular death in the cerebellar cortex after sub-chronic THC-20 administration. As expected, the CA3 region of the hippocampus in the positive control group showed Fluoro-Jade B staining corresponding to cellular death. Scale bars: 100  $\mu$ m (cerebellum), 50  $\mu$ m (hippocampus). **(B)** Representative double labeling for Iba1 (red) and Fluoro-Jade B (green) in sagittal cerebellar sections from sub-chronic VEH and sub-chronic THC-20 mice ( $n=3$  per group). Fluoro-Jade B reaction did not produce specific staining in the cerebellum of THC-20 treated mice. Scale bar: 25  $\mu$ m. **(C)** Immunoblot detection of Iba1 in cerebellar homogenates from mice exposed to sub-chronic THC-20 or VEH ( $n=5$  mice per group). Optical density analysis of Iba1 was referred to GAPDH detection in the same samples. **(D)** Immunolocalization of Iba1 in the cerebellar cortex of mice at the end of the sub-chronic THC-20 or VEH treatment. See inset for representative microglial morphological change. Iba1+ cells were counted in images representing an area of 0.8 mm<sup>2</sup> per optical field ( $n=4$  mice per group, 5 images per mouse). Scale bar: 100  $\mu$ m. **(E)** Immunoblot detection of glial fibrillary acidic protein (GFAP) in cerebellar homogenates from mice exposed to sub-chronic THC-20 or VEH ( $n=4$  per group). Optical density analysis of GFAP was referred to GAPDH detection in the same samples. **(F)** Immunohistochemical detection of GFAP after sub-chronic THC-20 or VEH exposure. Bright field images of stained sagittal cerebellar sections are presented in gray-scale for comparative purposes. All brain samples were collected 30 min after the last THC-20 or VEH administration ( $n=3$  mice per group). Scale bar: 100  $\mu$ m. **(G)** mRNA expression analysis by real time quantitative PCR of pro-inflammatory factors at the end of the sub-chronic THC-20 or VEH treatment ( $n=7-8$  per



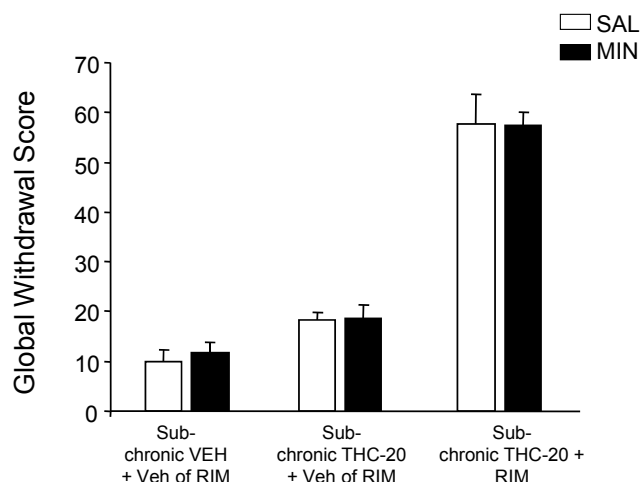
group). Cytokines mRNA levels were referred to GAPDH mRNA detection in the same samples. Abbreviations: ml: molecular layer; PC: Purkinje cell layer; gl: granular layer; CA3, CA3 field of Ammon's horn. Data were analyzed using one-way ANOVA and expressed as mean  $\pm$  SEM.



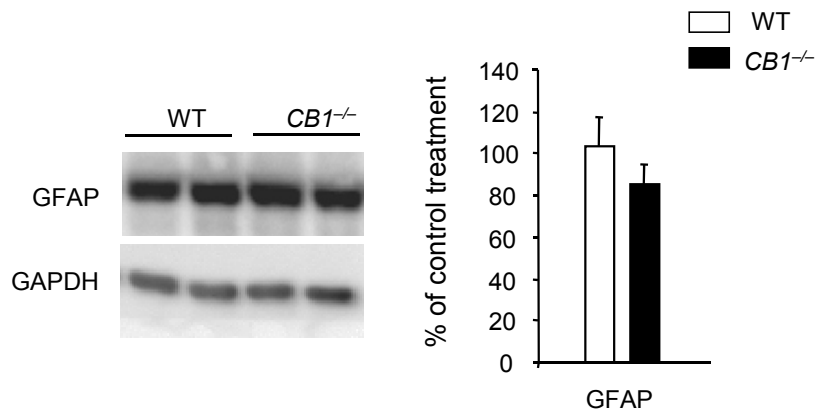
**Supplemental Figure 8.** Time course for the expression of CD11b, CB1R and the alteration in cerebellar microglia morphology during pharmacological treatment and after THC withdrawal. **(A)** Immunodetection and quantification for CD11b, CB1R and GAPDH on the same samples of cerebellar homogenates. Cerebellar tissues were obtained at different time points during the sub-chronic THC treatment (Day 3), at the end of the sub-chronic THC treatment (Day 6), 3 d after the end of sub-chronic THC treatment, and 5 d after the end of sub-chronic treatment. CD11b and CB1R expression was corrected by the detection of GAPDH. **(B)** Microglial morphology was analyzed on day 3 and 6 during sub-chronic treatment, and at day 3 and 5 after THC cessation. Confocal images were acquired and analyzed with the ImageJ software (Supplemental Figure 17). Scale bar: 25 µm. Data were expressed as mean ± SEM. ★p<0.05, ★★p<0.01, ★★★p<0.001 vs. sub-chronic VEH.



**Supplemental Figure 9.** CD11b+ (P4) population is highly enriched in Iba1+ cells. Staining for Iba1 and DAPI in CD11b+ (P4) and CD11b– (P5) cells sorted after acute dissociation of cerebellar tissue. Note that Iba1 staining appeared in CD11b+/DAPI+ cells, while it was not observed in CD11b–/DAPI+ cells. Scale bar: 25  $\mu$ m.



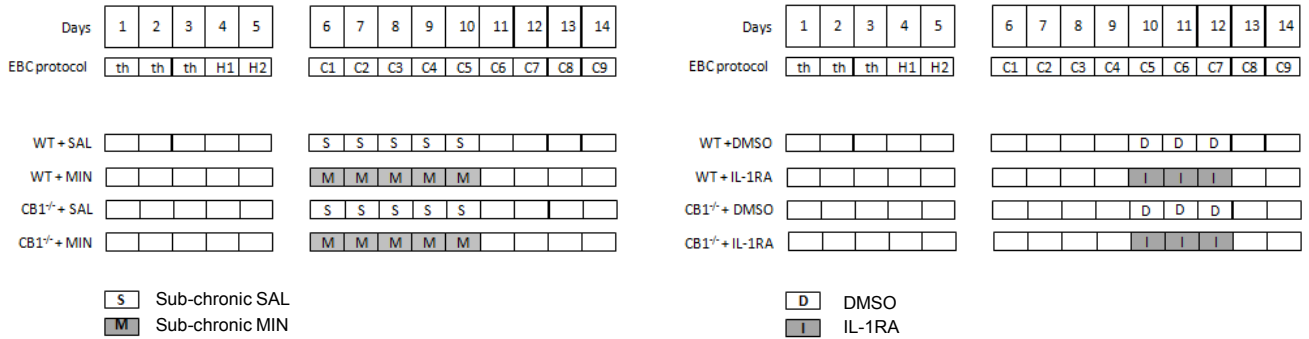
**Supplemental Figure 10.** Precipitated cannabinoid withdrawal syndrome is not affected by acute minocycline administration. Three hours after the last sub-chronic administration of THC (20 mg/kg, i.p.) or vehicle, mice received an administration of minocycline (MIN, 40 mg/kg, i.p.) or saline (SAL), and 1 hour later they were injected with rimonabant (RIM, 10 mg/kg, i.p.) or its vehicle (VEH) (n=10 mice per group). Then, mice were observed during 45 min and the somatic signs of withdrawal (paw tremor, wet dog shakes, sniffing, writhing, jumping, ptosis, piloerection, ataxia, mastication, locomotor activity, hunched posture and penil lick) were quantified. A global withdrawal score was obtained as described in the Methods section. RIM precipitated the characteristic cannabinoid withdrawal syndrome in mice treated sub-chronically with THC-20 and MIN administration did not alter the behavioral manifestations of cannabinoid withdrawal. Data were expressed as mean  $\pm$  SEM.



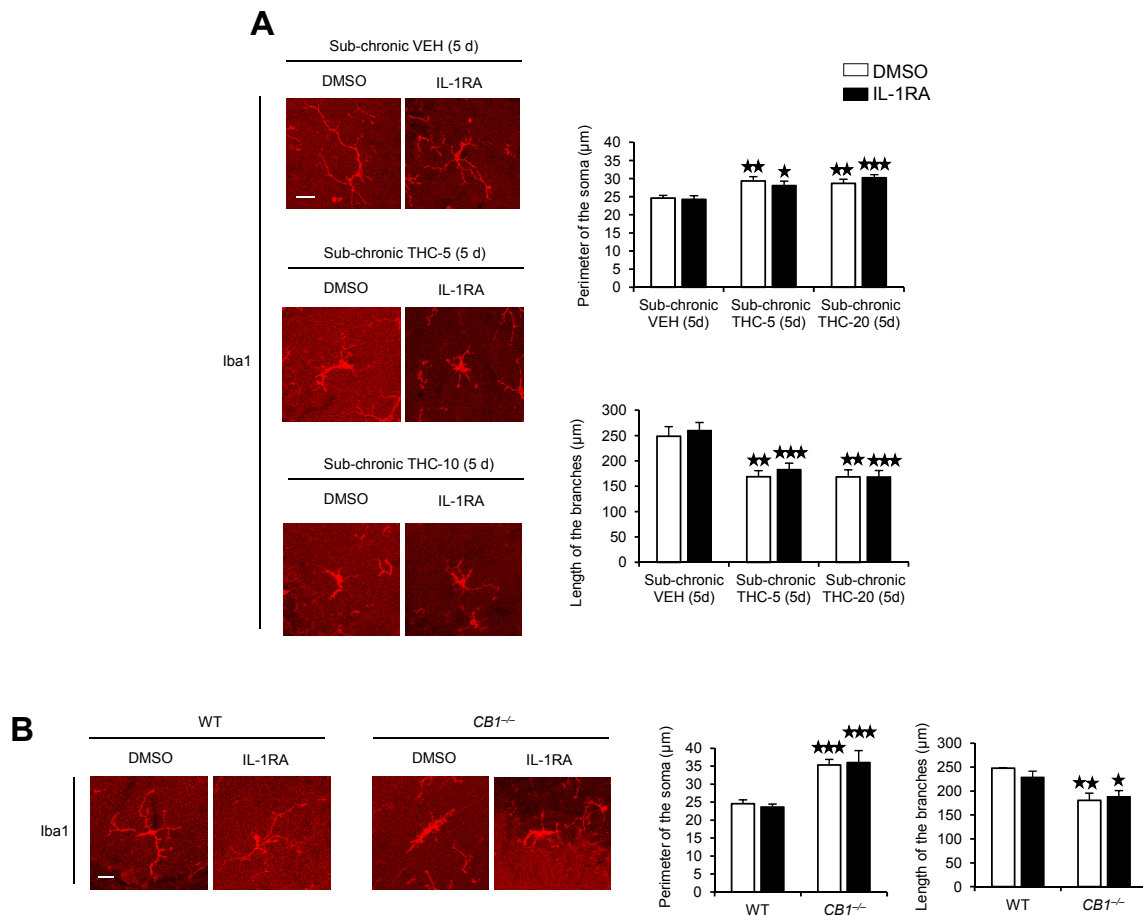
**Supplemental Figure 11.** Representative immunoblot and quantification of cerebellar GFAP in  $CB1^{-/-}$  line ( $n=6$  mice per group). No differences were observed in GFAP expression. Data were expressed as mean  $\pm$  SEM.

**A**

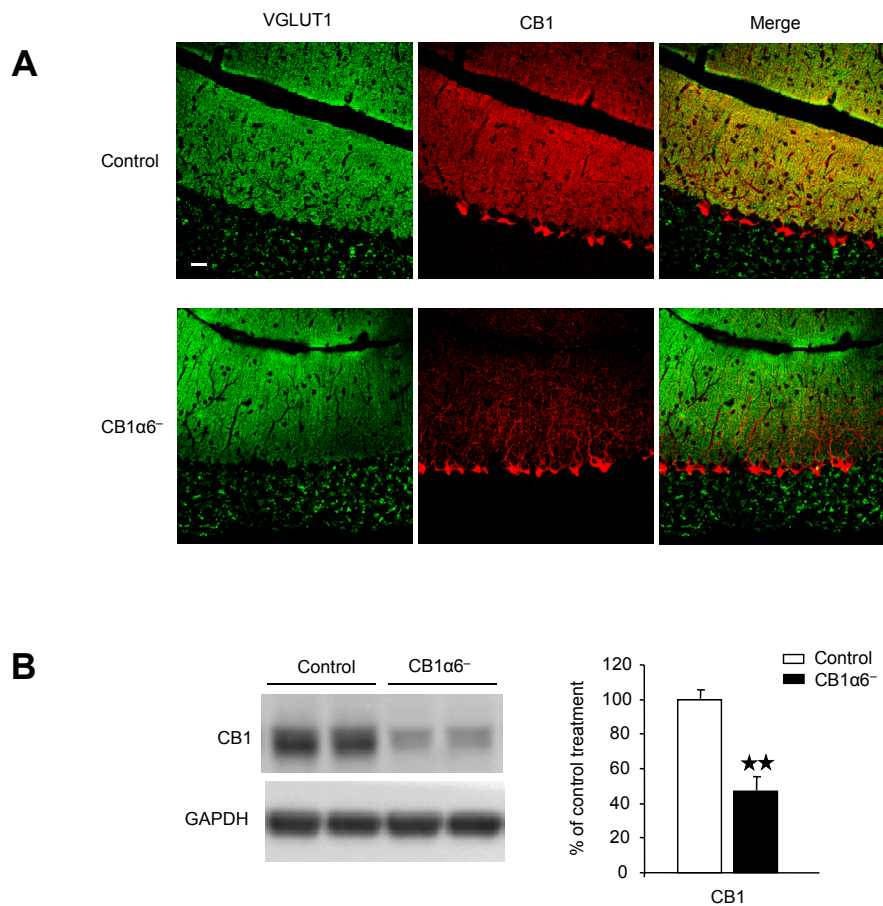
**B**



**Supplemental Figure 12.** Eyeblink conditioning schedules. **(A)** Chronogram for the experiments in Figure 5F. **(B)** Chronogram for the experiments in Figure 6B. Abbreviations: th, Search for thresholds; H, Habituation phase; C, Conditioning phase; T, THC; V, vehicle (VEH); M, minocycline (MIN); S, saline; I, IL-1RA; D, DMSO.

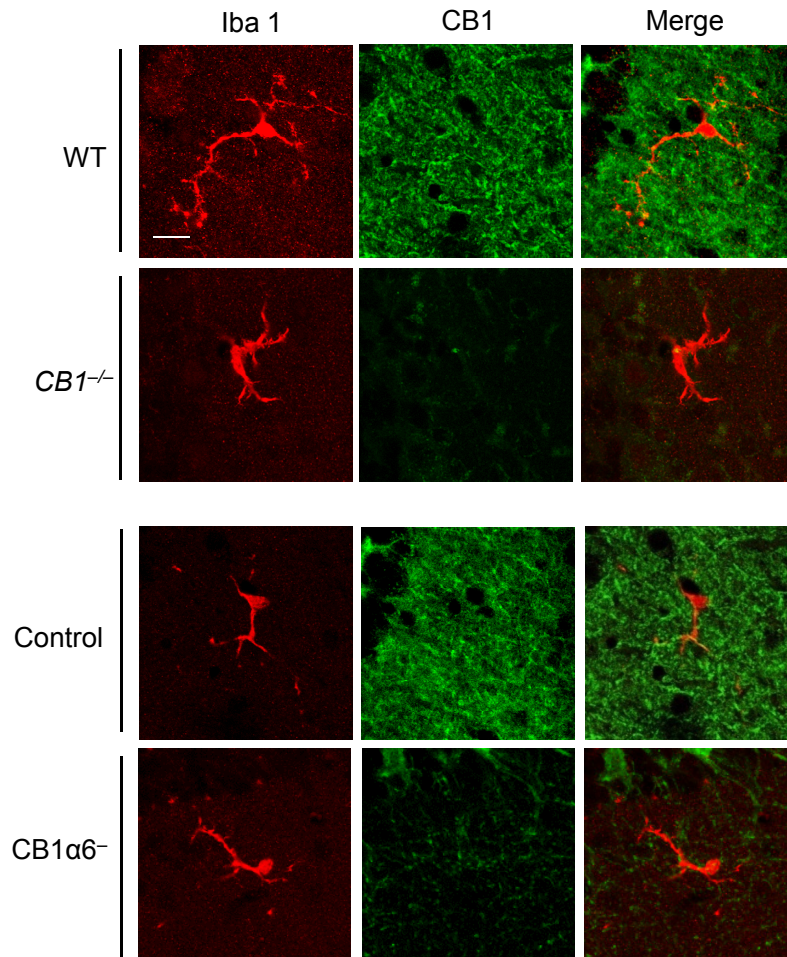


**Supplemental Figure 13.** IL-1RA acute administration does not modify microglial morphology. **(A)** The perimeter of the cell soma and the length of the microglial branches from Iba1-stained cells were analyzed in THC-withdrawn mice and VEH controls treated acutely with IL-1RA (100 mg/kg, i.p., 4h) or its vehicle (DMSO). Cerebellar sections were stained with Iba1 to reveal microglial morphology. Confocal images were analyzed with the ImageJ software as indicated in Supplemental Figure 17. Scale bar: 25  $\mu\text{m}$ . Data were expressed as mean  $\pm$  SEM.  $\star p < 0.05$ ,  $\star\star p < 0.01$ ,  $\star\star\star p < 0.001$  vs. sub-chronic VEH. **(B)** Analysis of the cerebellar microglial phenotype from  $CB1^{-/-}$  and WT mice after acute administration of IL-1RA (100 mg/kg, i.p., 4 h). Cerebellar sections were stained with Iba1 to reveal microglial morphology. Confocal images were analyzed with the ImageJ software as indicated in Supplemental Figure 17. Scale bar: 25  $\mu\text{m}$ . Data were expressed as mean  $\pm$  SEM.  $\star p < 0.05$ ,  $\star\star p < 0.01$ ,  $\star\star\star p < 0.001$  vs. WT+DMSO.

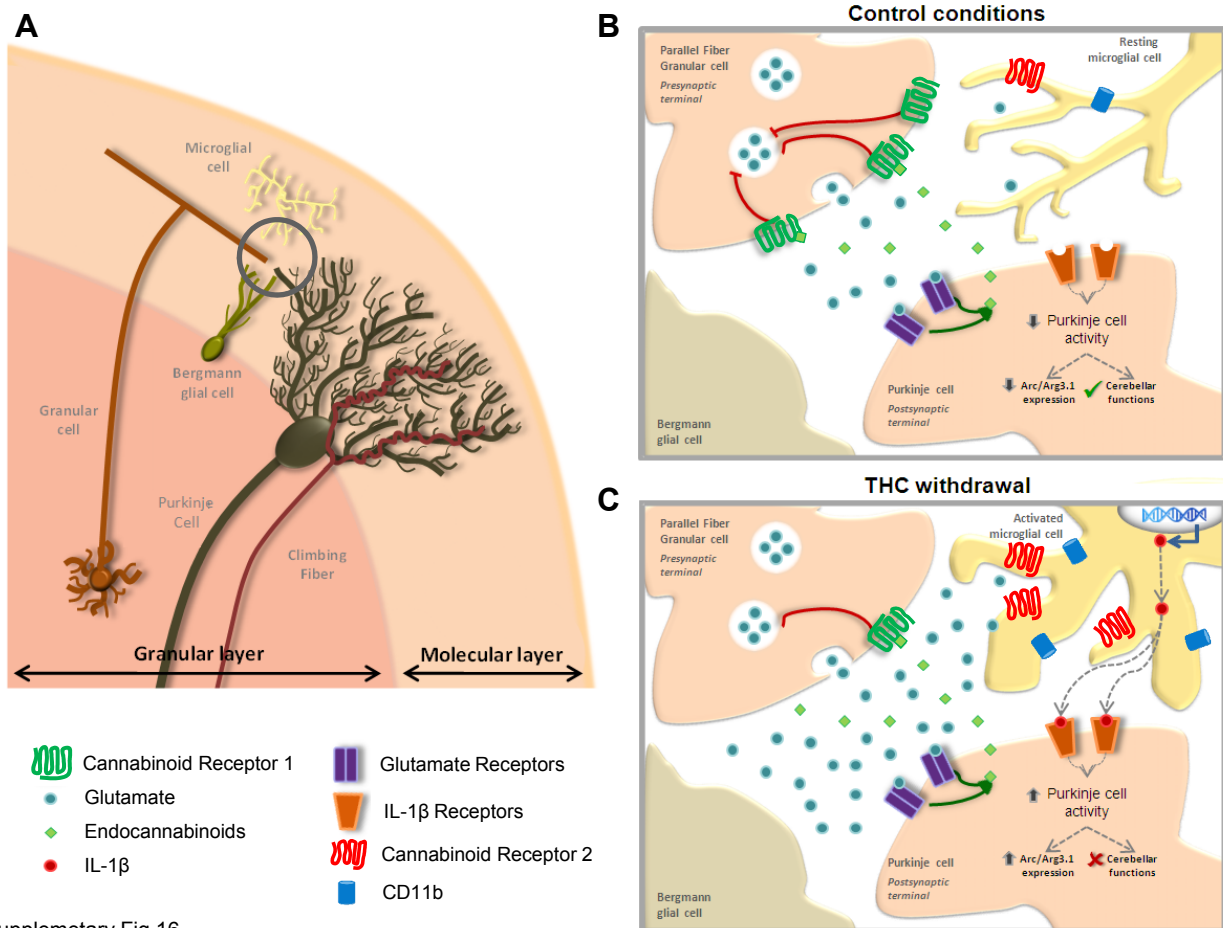


**Supplemental Figure 14.** Localization and expression of CB1R in the cerebellar cortex of CB1 $\alpha$ 6<sup>-</sup> line. **(A)** Immunofluorescence for VGLUT1 and CB1R in control and CB1 $\alpha$ 6<sup>-</sup> mice. Note the specific removal of CB1R in the parallel fibers on the molecular layer of the cerebellum in CB1 $\alpha$ 6<sup>-</sup> mice, without affecting VGLUT1 expression. Scale bar: 75  $\mu$ m. **(B)** Immunoblot detection and quantification of CB1R in cerebellar homogenates of control and CB1 $\alpha$ 6<sup>-</sup> mice ( $n=4$  mice per group). Data expressed as mean  $\pm$  SEM. **★★** $p < 0.01$  vs. control.



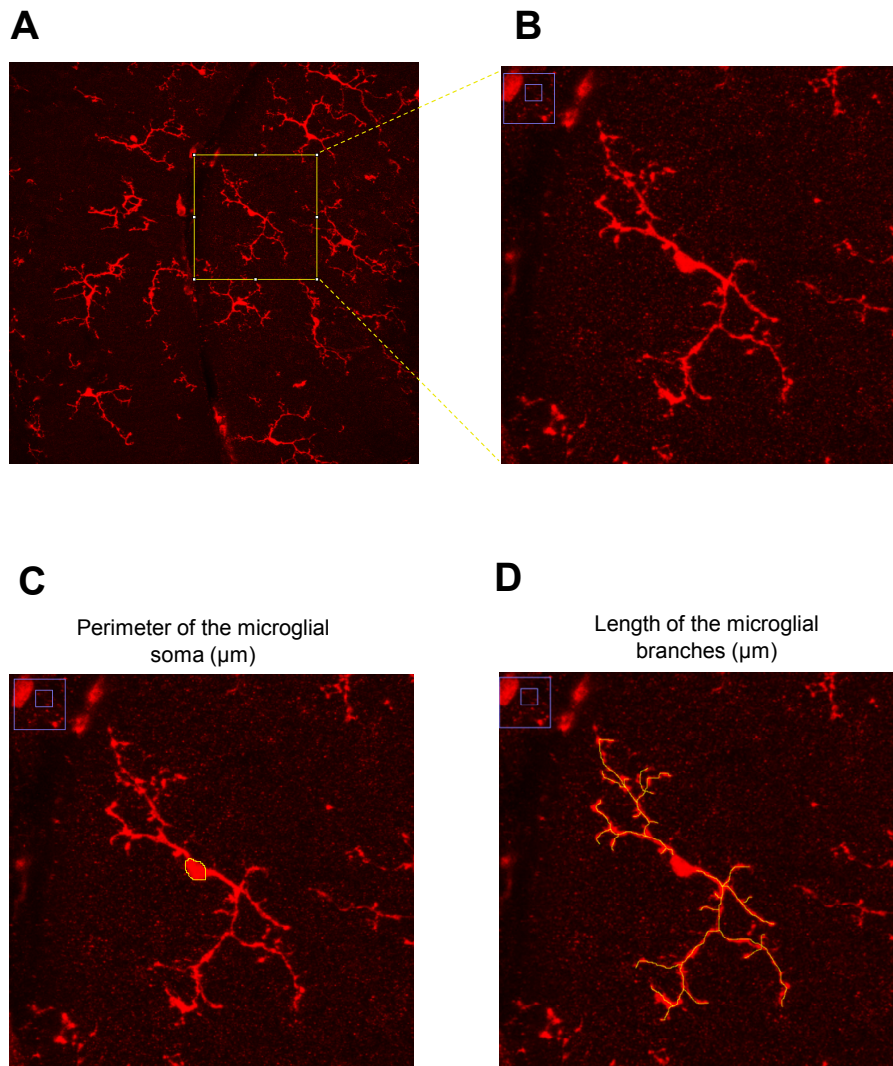


**Supplemental Figure 15.** Expression of low to undetectable levels of CB1R in microglial cells. Sections from WT, CB1<sup>-/-</sup>, control and CB1α6<sup>-</sup> mice were stained in parallel for CB1R and Iba1. CB1R signal was low to undetectable and did not change under neuroinflammatory conditions in Iba1<sup>+</sup> cells on CB1α6<sup>-</sup> mice. CB1<sup>-/-</sup> sections were used to determine the background signal of the assay. Scale bar: 25 μm.



Supplementary Fig.16

**Supplemental Figure 16.** Proposed model for the changes observed after sub-chronic THC exposure in the molecular layer of the cerebellum. **(A)** General organization of the main cellular components in the cerebellar cortex discussed in this study. **(B)** Under control conditions, CB1R located in the presynaptic parallel fibers modulate glutamatergic release in the Purkinje cell dendrites through highly ensheathed synapses. Quiescent microglial cells survey the synaptic and extrasynaptic gap. **(C)** After sub-chronic THC treatment –or genetic disruption of CB1R–, the CB1R down-regulation would result in the localized perturbation of glutamate handling. This glutamate de-regulation could enhance the activity of glutamate receptors expressed by microglial cells, promoting the classical activation characterized by morphological changes and enhancement in the CB2R and IL-1 $\beta$  transcription. IL-1 $\beta$  acting on the IL-1 receptors expressed in the Purkinje cell dendrites, could increase the Purkinje cell activity, as it was revealed by changes in Arc/Arg 3.1 expression. Activated microglia, alters cerebellar associative learning after sub-chronic THC exposure, and both, minocycline and IL-1R antagonist treatment, restore cerebellar function by reducing microglial activation and IL-1 $\beta$  action into the Purkinje cell, the main output of the cerebellar cortex.



**Supplemental Figure 17.** Methodology to measure microglial cell morphology in brain slices. (A) Images from Iba1 stained cells were acquired as Z-stacks (section of 15 $\mu$ m of with), to analyze the whole cell architecture. (B) Flattened images were examined by creating a region of interest (ROI) that would include the cell of interest entirely. The perimeter of the soma (C) and the length of the microglial branches (D) were measured using the ImageJ software tool “Freehand line”, as depicted. Afterwards, both parameters were recorded using the ImageJ software option “Analyze and Measure”.